
XYZ-IBD: A High-precision Bin-picking Dataset for Object 6D Pose Estimation Capturing Real-world Industrial Complexity

Junwen Huang

Technical University of Munich
Munich Center for Machine Learning
junwen.huang@tum.de

Jizhong Liang

Shanghai Jiaotong University
XYZ Robotics

Jiaqi Hu

Technical University of Munich

Martin Sundermeyer

Google
masundermeyer@google.com

Peter KT Yu

XYZ Robotics
peter.yu@xyzrobotics.com

Nassir Navab

Technical University of Munich
Munich Center for Machine Learning

Benjamin Busam

Technical University of Munich
Munich Center for Machine Learning
b.busam@tum.de

Abstract

We introduce XYZ-IBD, a bin-picking dataset for 6D pose estimation that captures real-world industrial complexity, including challenging object geometries, reflective materials, severe occlusions, and dense clutter. The dataset reflects authentic robotic manipulation scenarios with millimeter-accurate annotations. Unlike existing datasets that primarily focus on household objects, which approach saturation, XYZ-IBD represents the unsolved realistic industrial conditions. The dataset features 15 texture-less, metallic, and mostly symmetrical objects of varying shapes and sizes. These objects are heavily occluded and randomly arranged in bins with high density, replicating the challenges of real-world bin-picking. XYZ-IBD was collected using two high-precision industrial cameras and one commercially available camera, providing RGB, grayscale, and depth images. It contains 75 multi-view real-world scenes, along with a large-scale synthetic dataset rendered under simulated bin-picking conditions. We employ a meticulous annotation pipeline that includes anti-reflection spray, multi-view depth fusion, and semi-automatic annotation, achieving millimeter-level pose labeling accuracy required for industrial manipulation. Quantification in simulated environments confirms the reliability of the ground-truth annotations. We benchmark state-of-the-art methods on 2D detection, 6D pose estimation, and depth estimation tasks on our dataset, revealing significant performance degradation in our setups compared to current academic household benchmarks. By capturing the complexity of real-world bin-picking scenarios, XYZ-IBD introduces more realistic and challenging problems for future research. The dataset and benchmark are publicly available at <https://xyz-ibd.github.io/XYZ-IBD/>.

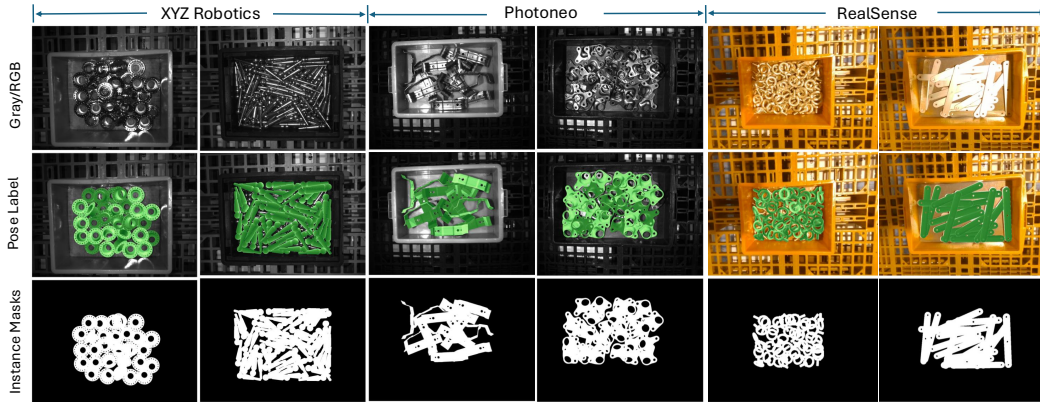


Figure 1: Example data from our industrial bin-picking dataset that shows challenging scenes captured by three cameras with different modalities, along with our 6D pose annotations.

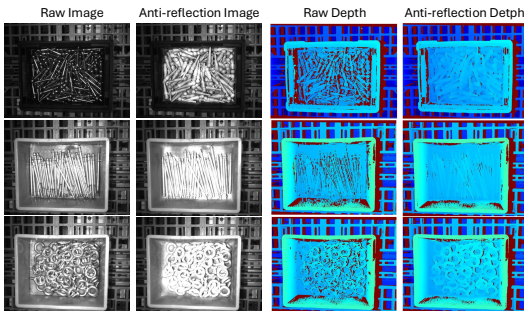


Figure 2: Comparison between raw depth and anti-reflection depth.



Figure 3: Example data of the synthetic training data with bin-picking simulation.

1 Introduction

The ability to detect, segment, and estimate the 6D pose of objects is critical for robotics applications, particularly in industrial bin-picking scenarios. These tasks demand not only high accuracy but also efficiency to enable real-time operation. While recent advancements in computer vision have significantly improved performance on benchmark datasets [1], there remains a substantial gap between academic research and real-world applications [2, 3]. This discrepancy is especially pronounced in industrial settings, where challenges such as clutter, occlusion, and reflective, texture-less objects must be addressed.

Current popular benchmarks for pose estimation, such as those designed for household objects [4–6], often exhibit favorable properties including rich textures, semantic cues, low occlusion, and minimal clutter. Some datasets [7–9] have extended the challenge by introducing texture-less objects [8], cluttered scenes [9], or robotic bin-picking setups [7]. While these household benchmarks have driven significant progress in pose estimation pipelines, state-of-the-art methods [10–12] still struggle with industrial objects that are highly reflective, symmetric, or lack distinctive visual features [13]. Unlike household objects, industrial items often lack contextual semantics and present ambiguous appearances, making them particularly difficult for feature extraction and accurate pose estimation, thereby the methods falling short of the precision requirements in real-world industrial manipulation. Although several datasets have begun to address these challenges by including texture-less, reflective, and symmetric industrial objects [8, 14–16], they still lack configurations that fully replicate the complexity of industrial bin-picking scenarios. These include randomly stacked objects in containers, harsh and variable lighting conditions, diverse object geometries, and multiple repeated instances with severe occlusion.

To address this need, we introduce XYZ-IBD, a novel RGB-D dataset specifically designed for industrial bin-picking applications. Unlike existing datasets, XYZ-IBD captures the complexity of real-world industrial environments, including challenging object geometries, severe scene clutter, and strong spectral reflections. The dataset features 15 texture-less, metallic, and mostly symmetric objects commonly used in industrial settings. As illustrated in Figure 1, these objects vary in shape and size, and are densely packed with multiple instances in cluttered bins, creating significant

occlusion. To ensure diverse and practical data modalities, we capture multi-view RGB and depth images using two high-precision industrial-grade cameras, an XYZ Robotic DLP structured light camera, and a Photoneo PhoXi laser scanner alongside a commercially available Intel RealSense D415 stereoscopic camera. The dataset consists of 75 real-world scenes (5 configurations per object), comprising over 22k labeled multi-view RGB-D frames and approximately 273k 6D pose annotations. Additionally, we provide a large-scale synthetic training set containing up to 45k rendered views generated using BlenderProc [17], simulating realistic bin-picking conditions through physics-based object interactions.

Given the millimeter-level precision required for industrial bin-picking, ensuring the accuracy of these annotations is essential. To provide accurate 6D pose annotations, we employ a multi-step, semi-automatic annotation pipeline. First, we sample and calibrate multiple viewpoints within a specified working distance using four calibration spheres. To enable precise depth map acquisition, we apply an anti-reflection spray to the objects, following practices from prior work [18–20]. We then fuse the depth data from multiple views using the high-quality ground truth depth. A self-developed annotation tool is used to label each object instance in the fused point cloud. Finally, the annotated object poses from the reference frame are projected to all remaining frames, followed by a manual double-check pass.

To quantify the accuracy of our pose annotations, we simulate real-world setups within a controlled simulation environment. We replicate the exact camera intrinsics and extrinsics used in our real-world experiments and randomly arrange objects in a virtual container. To closely mirror real-world conditions, we introduce camera measurement noise into the simulated images. The same annotation pipeline used for the real dataset is then applied to the simulated scenes. By comparing the resulting annotations to the ground truth poses available in the simulation, we compute the annotation error. This evaluation validates that our annotations are precise enough to serve as reliable ground truth for benchmarking 6D pose estimation methods. The overall data collection and annotation quantification is illustrated in Figure 4.

We benchmark XYZ-IBD on object 2D detection, object 6D pose estimation, and depth estimation tasks with state-of-the-art methods. While these methods perform exceptionally well on existing datasets, our experiments reveal a stark performance drop in the challenging conditions posed by XYZ-IBD. This highlights the current gap between recent academic benchmarks and real industrial conditions. By addressing the challenging scenarios, XYZ-IBD provides a much-needed benchmark for advancing detection, pose estimation, and depth estimation methods in realistic industrial settings. We firmly believe XYZ-IBD bridges the gap between current academic benchmarks and practical vision problems, fostering the development of more robust and efficient solutions for industrial robotics ultimately improving automation and machine support.

In summary, our key contributions are :

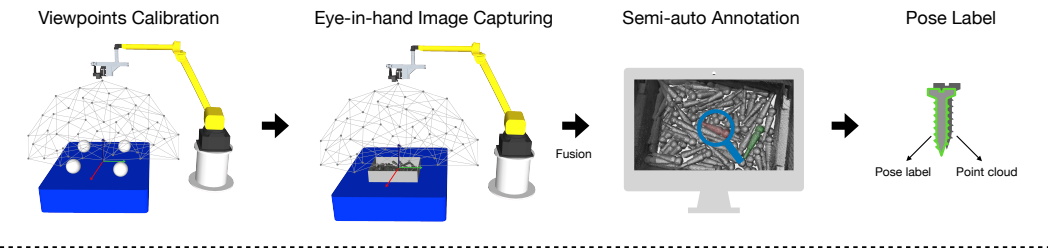
- We build a challenging real-world industrial bin-picking dataset that simultaneously captures the complexity of object geometry, material, occlusion, and clutter, introducing academic challenges for object detection and pose estimation tasks.
- Our dataset provides high-quality annotation for the industrial-grade demanded millimeter-level precision that provides accurate labels for multiple objective evaluation.
- We benchmark the dataset with 2D detection, 6D pose estimation, and depth estimation tasks with the most recent baselines, for both instance-specific and more generic frameworks.

2 Related Work

2.1 Household Datasets

A large number of object pose and scene depth datasets have been developed to address everyday scenarios involving household objects. Datasets such as LineMOD [21], LineMOD-Occlusion [9], YCB-V [4], HomebrewedDB [5], and TUD-L [6] are widely used in benchmarks for model-based object pose estimation [2, 6], and have driven progress on key challenges such as handling texture-less objects [21], occluded targets [9], and typical household environments [4, 5]. The HOPE dataset [22] extends this focus to robotic manipulation scenarios with varied lighting and occlusion conditions. IC-BIN [7] introduces an early bin-picking setup with randomly placed objects, but it includes

Real-world Data Acquisition



Annotation Quantification

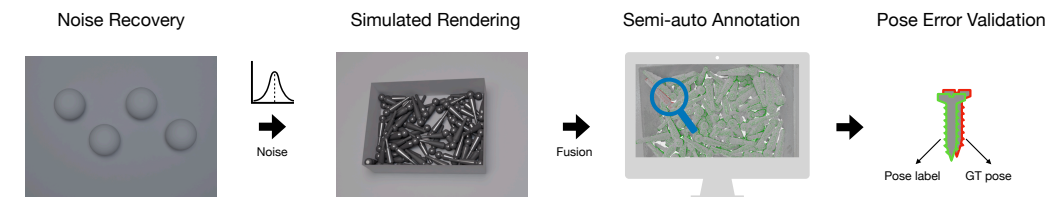


Figure 4: The real-world industrial data collection pipeline and the annotation error quantification pipeline in the simulated environment for XYZ-IBD dataset.

only two textured objects and suffers from low annotation quality. StereoOBJ-1M [15] improves annotation precision through structure-from-motion (SfM) with checkerboards and offers a large number of RGB images, yet it lacks object diversity and does not include depth data. NOCS [23] presents the first category-level 6D pose dataset, covering six household object categories. More recent datasets such as PhoCal [24], HouseCat6D [25], Booster [26], and SCREAM [20] focus on more complex scenes involving transparent or highly reflective objects and utilize a range of sensor modalities, including RGB, depth, and polarization images. While those datasets provide high-quality depth and pose annotations, they lack typical scene properties found in industrial environments. Therefore, existing datasets featuring household objects do not fully capture the challenges inherent in industrial applications, which involve both object-level and scene-level complexity.

2.2 Industrial Datasets

In industrial applications, the working environment is quite different from the household scenario. Firstly, unlike household objects, industrial parts are usually texture-less and often symmetric and highly reflective [13, 16, 18]. Consequently, networks trained on household objects hardly generalize to industrial datasets. Secondly, the required pose accuracy in industrial robotics is usually higher than in household robotics or AR/VR applications. The robotic arm is expected to not only pick up singulated objects, but typically needs to pick objects from a filled container and place them at a target pose or assemble them. Even though bin-picking is a typical setup for industrial applications, only a few publicly available datasets target this scenario which severely hampers the usability of pose estimation pipelines in industrial practice. T-LESS dataset [8] features texture-less industrial objects with symmetries but does not present challenging lighting conditions, and the annotation quality is not mm-accurate, a requirement in many industrial applications. Only a few scenes present the complexity of real bin-picking configurations where similar objects occlude each other. ITODD [13] collects industrial parts with challenging geometry and lighting conditions but does not feature bins filled with objects. The consistently low pose estimation scores on ITODD [13] in the BOP challenge [2] also demonstrate the need for industrial bin-picking datasets. Other datasets such as DIMO [14] and ROBI [18] focus on metallic objects for bin-picking setups, but they focus on a limited number of objects whose size and shape are not representative of the diversity in real applications. The recent dataset IPD [16] leverages multiple sensors to collect data from industrial objects but presents little clutter, stacking and occlusions which simplifies the setup compared to real industrial scenarios. Table 1 compares the characteristics of current industrial datasets.

Table 1: Comparison of datasets for object pose estimation from different dimensions.

Dataset	Modalities	Number of Objects	Object Diversity	Object Diameter (mm)	Frames	Instances	Instances per Scene	Accurate Depth GT	Occlusion	Reflection	Labeling Error (mm)
DIMO [14]	RGB-D	6	+	75~302	31.2k	100k	<10	✗	+	✗	2.7
FLESS [8]	RGB-D	30	+++	63~152	147k	100k	<10	✗	++	✗	11.3
ITODD [13]	RGB-D	28	+++	24~270	800	5k	<10	✗	++	✗	1.8
ROBI [15]	RGB-D	7	+	24~76	8k	600k	>10	✓	+++	✓	1.8
StereOBI-1M [15]	RGB	18	++	-	396k	1.5M	<10	✗	+	✗	2.3
IPD [16]	RGB-D+Polar	20	+++	80~240	30k	100k	<10	✗	+	✓	N/A
XYZ-IBD (Ours)	RGB-D	15	+++	54~300	22.5k	273k	22	✓	+++	✓	0.99

Table 2: Comparison of datasets with high-quality depth.

Dataset	Real Data	Camera Pose	Object Segmentation	Occlusion	Accurate Depth GT	No. Scenes	No. Frames
HAMMER [19]	✓	✓	✓	+	✓	13	~10k
PhoCal [19]	✓	✓	✓	+	✓	24	N/A
HouseCat6D [25]	✓	✓	✓	++	✓	41	~24k
Booster [26]	✓			+	✓	64	419
XYZ-IBD (Ours)	✓	✓	✓	+++	✓	75	~22k(+45k)

3 The XYZ-IBD Dataset

XYZ-IBD establishes a benchmark for industrial bin-picking by capturing data under authentic factory conditions. It advances prior work through four perspectives: **(1) Industrial-Grade Setup:** Data is acquired using industry-standard robotic arms (FANUC M10iD/8L) and multi-modal sensors (RGB/depth/grayscale) mounted at industrial working distances, replicating real application conditions. **(2) Challenging Objects:** 15 reflective, texturless, and mostly symmetric industrial parts that present rich geometrical shapes and sizes(54–300 mm scale), introducing academic challenges for pose estimation. **(3) Dense Clutter:** Objects are randomly and densely arranged in a container with multiple repeat instances, creating more ambiguity for instance detection and alignment. **(4) Precise Annotation:** Our annotation pipeline achieves <1 mm positional and <1° angular annotation accuracy, validated with simulated environment.

The dataset comprises 75 real-world scenes (5 configurations per object) with around 22k multi-view RGB-D frames, plus 45k synthetic images rendered using physics-based object interactions with BlenderProc [17], simulating the bin-picking setup.

3.1 Objects and Hardwares

Objects. Our dataset comprises 15 representative industrial parts with diameters ranging from 54 mm to 300 mm, including components like sheet metal parts, bolts, pins, covers, and many other kinds of machined metal objects. As shown in Figure 5 (b), these objects exhibit challenging visual properties such as high reflectivity and symmetry that are common in manufacturing environments yet problematic for vision algorithms. The original CAD models provided by industrial partners ensure micron-level geometric accuracy for both real-world captures and synthetic renderings. All real-world data is collected in bins with sensor-to-object distances carefully calibrated between 600-1000mm. We put multiple instances of each object into the bin, mostly with severe occlusion and clutter.

Sensor Setup. For precise and repeatable data acquisition, we employ an industrial-grade FANUC M10iD/8L robotic arm with ± 0.06 mm repeatability to position our multi-sensor array. Three complementary vision systems are rigidly co-mounted on the end-effector (see Figure 5 (a)): the *Intel RealSense D415 stereoscopic camera* provides aligned RGB (1920×1080) and depth streams at 30 FPS, offering baseline color-depth registration for general scene understanding; the *XYZ Robotic AL-M DLP structured-light camera* delivers high-precision grayscale (1440×1080) and depth maps (0.08mm resolution) through projected pattern deformation analysis, particularly effective for matte surfaces; the *Photoneo PhoXi M 3D scanner* utilizes laser triangulation to generate high-accuracy depth data (up to 2064×1544 resolution) with 0.1 mm voxel precision, complemented by synchronized grayscale imagery. All sensors are positioned at optimized working distances of 600-1000 mm based on object size and bin geometry, maintaining consistent fields-of-view across the industrial container. The fixed relative positions between cameras enable direct cross-modality calibration, while the robotic arm’s precise positioning ensures reproducible viewpoint acquisition throughout the data collection process.

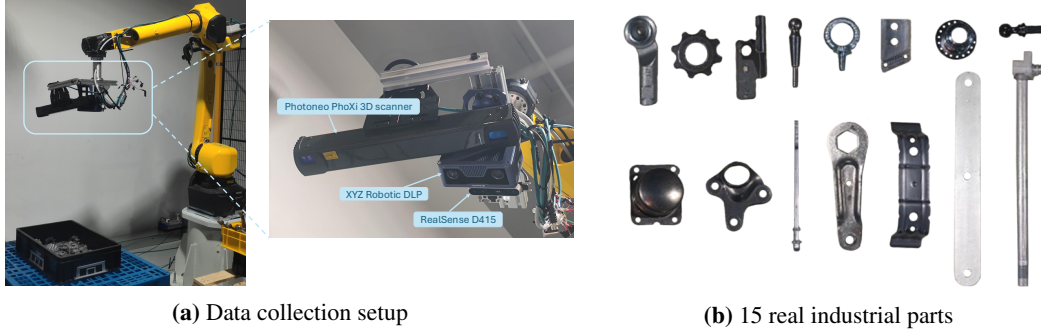


Figure 5: (a) shows the data collection setup for the robot arm and sensors; (b) lists the 15 real industrial parts used in XYZ-IBD dataset, showing the variance of the objects’ geometry and size.

3.2 Data Acquisition Pipeline.

As shown in Figure 4, our data acquisition pipeline integrates three sequential stages: viewpoint sampling and calibration, multi-pass scene capture for depth ground truth, and a hybrid annotation protocol combining manual and algorithmic refinement.

Multi-view Sampling and Calibration. Beginning with the bin’s centroid as the origin, we define a spherical sampling surface spanning elevation angles of 45° to 90° to balance perspective diversity and robotic arm operability. Fifty viewpoints are randomly distributed across this surface to ensure comprehensive spatial coverage. Following the calibration framework of [18], we place four precisely machined calibration spheres on the working plane. During an initial calibration pass, the robotic arm captures multi-modal images of these spheres across all viewpoints. The cameras are firstly undistorted and obtain the initial camera poses with hand-eye calibration [27], then pose refinement via iterative closest point (ICP) alignment on the spheres’ point clouds establishes relative transformations between viewpoints with around 0.248 mm average root mean square error (RMSE), resolving the 6 DoF relationships between 49 secondary viewpoints and a primary reference view. These transformations enable subsequent multi-view data fusion and label projection with sub-millimeter consistency. After calibration, the calibration spheres are removed, and the robotic arm systematically revisits each pre-calibrated viewpoint to capture cluttered industrial bin-picking scenes. At each viewpoint, three rigidly mounted cameras (Intel RealSense D415, XYZ Robotic DLP, Photoneo PhoXi) acquire synchronized RGB, grayscale, and depth data. To maximize scene diversity, we perform five complete capture cycles per object, randomly shuffling parts between cycles.

Multi-Pass Scene Capture. To address depth sensing challenges from reflective surfaces, we employ a dual-phase capture strategy. The first phase applies a temporary anti-reflective coating (Acksys SP-102) to suppress specularities, enabling high-fidelity ground truth depth acquisition. After allowing 15 minutes for complete evaporation under controlled ambient conditions ($25^\circ\text{C} \pm 1^\circ\text{C}$), we execute an identical second capture pass to record the scene’s native optical properties. Both phases maintain pixel-wise spatial correspondence through robotic arm pose repetition (± 0.06 mm precision), providing high-quality depth to fuse the scene point cloud, thus resulting in more accurate pose annotation and also aligned datasets of enhanced and raw depth for algorithm benchmarking.

6D Pose Annotation. The annotation derives from a hierarchical process beginning with 3D fusion of spray-enhanced depth data into a unified scene point cloud. Annotators coarsely align CAD models to this reconstruction using our developed constrained GUI (± 1 mm translational, $\pm 1^\circ$ rotational increments), followed by multi-scale ICP refinement. The ICP pipeline first aligns downsampled point clouds for global adjustment and then iteratively optimizes with full-resolution data to achieve sub-millimeter accuracy. Finalized poses are propagated to all 50 viewpoints using pre-calibrated transformations that we obtained from the first stage, ensuring label consistency across perspectives without manual per-view annotation. This protocol yields around 273k annotated object instances in total, with a minimum of 11 and a maximum of 60 instances per scene, resulting in an average of 22 instances per image. We choose the XYZ Robotic DLP camera as the primary camera and perform annotations on the data it collected. The annotation of the other two cameras are projected through the calibrated relative transformation between the cameras.

Table 3: Specifications for data collection error sources.

Source	Specify	Error (mm)
Viewpoints Calibration	Sensor Calibration	0.10
	Sensor Temporal noise	0.10
	Sensor Distortion	N/A
	Robot arm Repeatability	0.06
	Viewpoints Calibration RMSE (Total)	0.245
Depth fusion	TSDf	N/A
Manually annotate	Human, ICP	N/A
Overall		0.99

Table 4: Effect of Gaussian noise on average viewpoints calibration RMSE.

Gaussian Noise σ (mm)	RMSE (mm)
0.0	0.199
0.1	0.209
0.2	0.233
0.26	0.248
0.3	0.259

3.3 Annotation Error Quantification.

To quantify the cumulative annotation error, we replicated the data collection and annotation process in a simulated environment, recovering the sensor error, calibration error and the human annotation error, and compared the resulting annotations against ground truth poses. Our evaluation framework comprises three stages: data noise recovery, synthetic data collection, and 6D pose quantification.

Data Noise Recovery. We simulate the multi-view calibration procedure in a synthetic environment using identical calibration spheres and camera parameters as in the real-world setup. 50 calibration views are sampled, and varying levels of Gaussian noise are added to the rendered depth images. The corresponding RMSE of the point cloud is then computed using ICP, revealing the relationship between noise magnitude and calibration error (see Table 4). When Gaussian noise $\sigma = 0.26$ mm is applied, the computed RMSE reached 0.248 mm, matching the error observed during real-world calibration. This provided the chosen noise level to best represent the cumulative error introduced by the sensor, robotic system, and multi-view calibration process.

Synthetic Data Collection. To ensure realistic, cluttered arrangements, we generate synthetic counterparts using the same CAD models within a simulated bin-picking environment rendered with physically-based rendering in BlenderProc [17]. Objects are randomly dropped into the bin via a free-fall simulation, and any that fall outside the bin are removed. Multi-view synthetic images are rendered using a complementary noise model derived in the last step. The same annotation pipeline used for real data, incorporating multi-view fusion, manual adjustments, and multi-scale ICP refinement, is also applied to the synthetic scenes. As ground truth poses are available in the simulation, this setup allows for direct comparison between annotated and true object poses.

To complement the real dataset, we additionally render a large-scale synthetic dataset as the training data. We programmatically vary rendering conditions, including lighting, material properties, object quantity, and pose configurations, closely replicating real-world setups to ensure cross-domain consistency. For each of the 15 objects, we perform 120 free-fall simulations, with random variations in material and lighting, resulting in a total of approximately 45,000 frames in the synthetic training dataset. As shown in Figure 3, this parallel real-synthetic collection supports robust benchmarking while preserving strong visual alignment between domains.

6D Pose Quantification. To assess annotation quality, we systematically investigated several error sources: inherent sensor inaccuracies, robotic arm repeatability, viewpoint calibration discrepancies, and annotator subjectivity. Specifically, the sensor error encompasses both the camera calibration inaccuracies and measurement noise due to sensor characteristics and environmental conditions. This, together with the robot arm repeatability, is manifested in the overall multi-view pose calibration error. We compute pose errors through nearest-neighbor matching between annotated and GT poses using Hungarian assignment on 3D centroid distances. We analyze up to 60 samples per scene \times 3 scenes per object, revealing a mean positional error of 0.999 mm ($\sigma = 0.12$ mm) and an angular error of 0.432° ($\sigma = 0.08^\circ$). Per-object error averages across 15 industrial parts demonstrate sub-millimeter precision even for challenging geometries. This synthetic validation confirms that our real-world annotations achieve <1 mm positional and $<1^\circ$ angular accuracy relative to physical GT.

4 Benchmarks

Our dataset provides high-precision 6D object pose and depth annotations, enabling the establishment of a comprehensive benchmark for object detection, pose estimation, and depth estimation. The XYZ-IBD dataset is included as one of the official pose estimation datasets in the industrial track of the BOP Challenge 2025 [3], and as one of the depth estimation datasets in the monocular depth

track of TRICKY Challenge 2025 [28]. To ensure consistency with these challenges, we adopt their evaluation metrics to assess performance on our dataset. For the 2D detection and 6D pose estimation tasks, we evaluate representative methods under both seen and unseen object settings. In the seen object setup, models are trained on our synthetic dataset and evaluated on the real-world test split. In the unseen object setup, we directly apply off-the-shelf generalizable methods, which have been pretrained on large-scale external datasets, to our real test scenes. We benchmark several recent state-of-the-art methods across all three tasks. Detailed implementation settings for these baseline methods are provided in the Supplemental Material.

4.1 Evaluation Criteria

Object 2D Detection Metrics. For the object 2D detection task, we follow the model-based 2D detection task defined in BOP 2024-2025 Challenge [2]. The objective is to generate a set of non-overlapping 2D binary instance masks with associated confidence scores from an RGB-D input image that contains multiple object instances from a given dataset. To evaluate performance, we adopt the Average Precision (AP) metric, following the protocol used in the COCO 2020 challenges [29]. AP is calculated by averaging the precision scores at several Intersection-over-Union (IoU) thresholds, ranging from 0.5 to 0.95 in increments of 0.05. Each object’s AP score reflects its detection quality across these thresholds. To obtain an overall dataset-level performance measure, the *mean Average Precision (mAP)* is computed by averaging the AP scores across all object categories. This evaluation strategy comprehensively captures both the accuracy of object localization and the effectiveness of category-level recognition, ensuring alignment with established benchmarking standards.

Object 6D Pose Estimation Metrics. For the 6D pose estimation task, we adopt the model-based 6D object detection metric defined in BOP 2024-2025 Challenge [2], evaluating detection accuracy using symmetry-aware Average Precision (AP) scores. For each predicted pose \hat{P} and its corresponding ground truth pose P_{GT} , we compute two error metrics: *Maximum Symmetry-Aware Surface Distance (MSSD)* and *Maximum Symmetry-Aware Projection Distance (MSPD)*. MSSD measures the maximum 3D surface deviation under object symmetries, defined as $e_{MSSD} = \max_{x \in M} \min_{S \in \mathcal{S}} |\hat{P}x - S(P_{GT}x)|$, where M is the object mesh and S is the set of predefined symmetry transformations. MSPD evaluates the maximum 2D projection deviation considering object symmetries, computed as $e_{MSPD} = \max_{u \in U} \min_{S \in \mathcal{S}} |\Pi(\hat{P}x_u) - \Pi(S(P_{GT}x_u))|$, where Π denotes the camera projection function and U the set of visible mesh vertices. A pose estimate is deemed correct when the error e falls below a threshold θ_e . For each error type $e \in \{MSSD, MSPD\}$ and object $o \in O$, we compute the object-level AP score as $AP_{e,o} = \frac{1}{|\Theta_e|} \sum_{\theta \in \Theta_e} P_o(\theta)$, where Θ_e is the set of threshold values and $P_o(\theta)$ is the precision at threshold θ . The final AP score aggregates over all objects and both error types as $AP = \frac{1}{2|O|} \sum_{o \in O} \sum_{e \in \{MSSD, MSPD\}} AP_{e,o}$.

Monocular Depth Estimation Metrics. We evaluate monocular depth predictions following the benchmark in TRICKY Challenge (Transparent & Reflective objects In the wild Challenges) [26, 30, 31]. Since monocular networks estimate depth up to an unknown scale, we first align the predicted and ground truth depths by applying a shift and scale transformation to match their value ranges. We then compute several evaluation metrics: the *Absolute Relative Error (AbsRel)*, the *Mean Absolute Error (MAE)*, and the *Root Mean Squared Error (RMSE)*. Additionally, we measure the percentage of pixels where the percentage of pixels having the maximum between the prediction and ground-truth ratios is lower than a threshold, denoted as δ_i , with $i = 1.05$. All metrics are computed over three pixel subsets: (1) *All* valid pixels, (2) pixels belonging to Transparent or Mirror surfaces (Class *ToM*), and (3) pixels belonging to other material types (Class *Other*). Lower values of AbsRel, MAE, and RMSE indicate better performance, whereas higher δ_i scores are preferred.

Table 5: Comparison of baseline performance on **object 2D detection** and **6D pose estimation** tasks.

Task	2D Detection			6D Detection			
Seen Object	✓	✗		✓	✗		
Methods	YOLOX [32]	CNOS [33]	SAMD	GDRNet [12]	SurfEmb [34]	SAM-6D [11]	FoundationPose [10]
mAP	0.774	0.275	0.296	0.266	0.274	0.438	0.547

4.2 Evaluation of Object 2D Detection

YOLOX [32] (Seen) is a widely used advanced real-time object detection model that builds upon the YOLO [35] series. We follow the implementation of GDRNet [12] to train the model on our

Table 6: Evaluation on **monocular depth estimation** on our dataset with Depth Anything V2 [40].

CLASS	$\delta_{1.05}$	MAE (mm)	AbsRel (%)	RMSE (mm)
<i>All</i>	78.05	26.4	3.46	41.8
<i>TOM</i>	85.08	19.3	2.76	22.3
<i>Other</i>	74.87	29.8	3.78	48.5

synthetic training data and test on the real-world images. **CNOS** [33] (Unseen) is a model-based method that uses vision foundation models SAM [36] and DINOv2 [37] for novel object segmentation and detection without re-training. It renders object templates from a CAD model and ranks SAM-generated segments by comparing their DINOv2 class token features with those of the templates. **SAM-6D** [11] (Unseen) detects the objects with a similar strategy as CNOS [33] but computes a weighted score including semantics, appearance, and geometry to match the query object template with the segments extracted from SAM [36].

As shown in Table 5, for the 2D detection task, YOLOX [32], trained on our synthetic training split, achieves over 77% mAP on the real test set. In contrast, generic methods such as CNOS and SAM-6D, which are not trained on the specific objects, exhibit a significant drop in performance. These results highlight the increased difficulty of our dataset for 2D detection, due to heavy occlusion, repeated object instances, and strong surface reflections.

4.3 Evaluation of Object 6D Detection

SurfEmb [34] (Seen) learns per-object dense 2D–3D correspondence distributions over object surfaces using contrastive learning in an unsupervised fashion. It achieves strong performance on BOP and handles visual ambiguities effectively. **GDRNet** [12] (Seen) is a recent state-of-the-art framework that processes zoomed-in RoIs from RGB images to predict intermediate geometric features: dense 2D-3D correspondences, surface region attention maps, and visible object masks. These features guide a Patch-PnP module to directly regress the 6D pose in a differentiable manner. **FoundationPose** [10] (Unseen) supports both model-based and model-free settings using neural implicit representations for view synthesis. Trained on large-scale synthetic data with transformer-based coarse-to-fine design, it generalizes well and outperforms prior methods across benchmarks. **SAM-6D** [11] (Unseen) uses the Segment Anything Model for segmentation and applies ViT [38] and GeoTransformer [39] to extract features from RGB-D input and CAD models. Trained on a large-scale synthetic dataset, it achieves strong performance in model-based 6D pose estimation.

Unseen object methods assume the availability of object segmentation or detection as a prior for pose estimation. Accordingly, we use segmentation masks produced by SAM-6D for fair comparison among these methods, while seen object methods utilize detection results from YOLOX. As shown in Table 5, all methods struggle on our dataset. Specifically, both GDRNet and SurfEmb, representing seen object methods, fail to predict accurate poses, despite being trained on synthetic data. In contrast, unseen object methods demonstrate relatively better performance, with FoundationPose achieving state-of-the-art results. Compared to existing benchmarks based on household objects [2, 1], our dataset introduces greater challenges for pose estimation due to the complexity of object materials, geometric variations, and severe scene clutter.

4.4 Depth Estimation

We evaluate the recent state-of-the-art depth estimation framework **Depth Anything V2** [40] on our dataset. We test the Base model (97.5M) and report the detailed metrics in Table 6. While Depth Anything V2 demonstrates strong performance on other scene-scale benchmarks, its depth prediction error on XYZ-IBD reveals a gap relative to the millimeter-level precision required for industrial applications involving small-scale objects.

5 Conclusion and Limitations

In this paper, we introduce the XYZ-IBD dataset, a high-precision bin-picking dataset that captures real-world industrial-grade complexity, including object reflectivity, scene clutter, and heavy occlusion. The dataset comprises 15 industrial parts collected under real factory conditions using three different sensors, resulting in 273k real-world annotated samples, along with a 45k-frame synthetic dataset

simulating realistic bin-picking environments. Through a multi-stage, semi-automatic protocol, XYZ-IBD provides accurate 6D pose annotations, with error quantified via simulations that model real-world sensor and calibration noise, achieving pose errors as low as 1 mm. The dataset is actively integrated into ongoing challenges, including the BOP Challenge 2025 (Industrial Track) and the TRICKY Challenge 2025 (Monocular Depth Track). We believe XYZ-IBD brings real-world industrial vision problems to the academic community and helps bridge the gap between academic research and practical application. While we focus on a specific industrial scenario for bin-picking, the working distance and the scale of the objects are still limited, which is a potential limitation for the methods to generalize to other objects with different materials and shapes.

References

- [1] M. Sundermeyer, T. Hodaň, Y. Labbe, G. Wang, E. Brachmann, B. Drost, C. Rother, and J. Matas, “Bop challenge 2022 on detection, segmentation and pose estimation of specific rigid objects,” in *CVPR*, 2023.
- [2] N. Van Nguyen, S. Tyree, A. Guo, M. Fourmy, A. Gouda, T. Lee, S. Moon, H. Son, L. Ranftl, J. Tremblay *et al.*, “Bop challenge 2024 on model-based and model-free 6d object pose estimation,” *arXiv e-prints*, pp. arXiv–2504, 2025.
- [3] [Online]. Available: <https://bop.felk.cvut.cz/challenges/>
- [4] Y. Xiang, T. Schmidt, V. Narayanan, and D. , “Posecnn: A convolutional neural network for 6d object pose estimation in cluttered scenes,” *Robotics: Science and Systems*, 2018.
- [5] R. Kaskman, S. Zakharov, I. Shugurov, and S. Ilic, “Homebreweddb: Rgb-d dataset for 6d pose estimation of 3d objects,” *ICCVW*, 2019.
- [6] T. Hodan, F. Michel, E. Brachmann, W. Kehl, A. GlentBuch, D. Kraft, B. Drost, J. Vidal, S. Ihrke, X. Zabulis, C. Sahin, F. Manhardt, F. Tombari, T.-K. Kim, J. Matas, and C. Rother, “Bop: Benchmark for 6d object pose estimation,” in *ECCV*, 2018.
- [7] A. Doumanoglou, R. Kouskouridas, S. Malassiotis, and T.-K. Kim, “Recovering 6d object pose and predicting next-best-view in the crowd,” in *Proceedings of the IEEE conference on computer vision and pattern recognition*, 2016, pp. 3583–3592.
- [8] T. Hodaň, P. Haluza, Š. Obdržálek, J. Matas, M. Lourakis, and X. Zabulis, “T-LESS: An RGB-D dataset for 6D pose estimation of texture-less objects,” *WACV*, 2017.
- [9] E. Brachmann, A. Krull, F. Michel, S. Gumhold, J. Shotton, and C. Rother, “Learning 6d object pose estimation using 3d object coordinates,” in *ECCV*, 2014.
- [10] B. Wen, W. Yang, J. Kautz, and S. Birchfield, “Foundationpose: Unified 6d pose estimation and tracking of novel objects,” in *Proceedings of the IEEE/CVF Conference on Computer Vision and Pattern Recognition*, 2024, pp. 17 868–17 879.
- [11] J. Lin, L. Liu, D. Lu, and K. Jia, “Sam-6d: Segment anything model meets zero-shot 6d object pose estimation,” in *Proceedings of the IEEE/CVF Conference on Computer Vision and Pattern Recognition*, 2024, pp. 27 906–27 916.
- [12] G. Wang, F. Manhardt, F. Tombari, and X. Ji, “Gdr-net: Geometry-guided direct regression network for monocular 6d object pose estimation,” in *CVPR*, 2021.
- [13] B. Drost, M. Ulrich, P. Bergmann, P. Hartinger, and C. Steger, “Introducing mvtec itodd - a dataset for 3d object recognition in industry,” in *ICCVW*, 2017.
- [14] P. De Roovere, S. Moonen, N. Michiels, and F. Wyffels, “Dataset of industrial metal objects,” *arXiv preprint arXiv:2208.04052*, 2022.
- [15] X. Liu, S. Iwase, and K. M. Kitani, “Stereobj-1m: Large-scale stereo image dataset for 6d object pose estimation,” in *Proceedings of the IEEE/CVF international conference on computer vision*, 2021, pp. 10 870–10 879.
- [16] A. Kalra, G. Stoppi, D. Marin, V. Taamazyan, A. Shandilya, R. Agarwal, A. Boykov, T. H. Chong, and M. Stark, “Towards co-evaluation of cameras hdr and algorithms for industrial-grade 6dof pose estimation,” in *Proceedings of the IEEE/CVF Conference on Computer Vision and Pattern Recognition (CVPR)*, June 2024, pp. 22 691–22 701.

- [17] M. Denninger, M. Sundermeyer, D. Winkelbauer, D. Olefir, T. Hodan, Y. Zidan, M. Elbadrawy, M. Knauer, H. Katam, and A. Lodhi, “Blenderproc: Reducing the reality gap with photorealistic rendering,” in *International Conference on Robotics: Science and Systems(RSS)*, 2020.
- [18] J. Yang, Y. Gao, D. Li, and S. L. Waslander, “Robi: A multi-view dataset for reflective objects in robotic bin-picking,” in *2021 IEEE/RSJ International Conference on Intelligent Robots and Systems (IROS)*. IEEE, 2021, pp. 9788–9795.
- [19] H. Jung, P. Ruhkamp, G. Zhai, N. Brasch, Y. Li, Y. Verdie, J. Song, Y. Zhou, A. Armagan, S. Ilic *et al.*, “On the importance of accurate geometry data for dense 3d vision tasks,” in *Proceedings of the IEEE/CVF Conference on Computer Vision and Pattern Recognition*, 2023, pp. 780–791.
- [20] H. Jung, W. Li, S.-C. Wu, W. Bittner, N. Brasch, J. Song, E. Pérez-Pellitero, Z. Zhang, A. Moreau, N. Navab, and B. Busam, “SCRREAM : SCAn, register, REndeR and map: A framework for annotating accurate and dense 3d indoor scenes with a benchmark,” in *The Thirty-eight Conference on Neural Information Processing Systems Datasets and Benchmarks Track*, 2024. [Online]. Available: <https://openreview.net/forum?id=NHob4eMg7R>
- [21] S. Hinterstoisser, V. Lepetit, S. Ilic, S. Holzer, G. Bradski, K. Konolige, and N. Navab, “Model based training, detection and pose estimation of texture-less 3d objects in heavily cluttered scenes,” in *Asian conference on computer vision*. Springer, 2012, pp. 548–562.
- [22] S. Tyree, J. Tremblay, T. To, J. Cheng, T. Mosier, J. Smith, and S. Birchfield, “6-dof pose estimation of household objects for robotic manipulation: An accessible dataset and benchmark,” in *2022 IEEE/RSJ International Conference on Intelligent Robots and Systems (IROS)*. IEEE, 2022, pp. 13 081–13 088.
- [23] H. Wang, S. Sridhar, J. Huang, J. Valentin, S. Song, and L. J. Guibas, “Normalized object coordinate space for category-level 6d object pose and size estimation,” in *Proceedings of the IEEE/CVF conference on computer vision and pattern recognition*, 2019, pp. 2642–2651.
- [24] P. Wang, H. Jung, Y. Li, S. Shen, R. P. Srikanth, L. Garattoni, S. Meier, N. Navab, and B. Busam, “Phocal: A multi-modal dataset for category-level object pose estimation with photometrically challenging objects,” in *Proceedings of the IEEE/CVF conference on computer vision and pattern recognition*, 2022, pp. 21 222–21 231.
- [25] H. Jung, S.-C. Wu, P. Ruhkamp, H. Schieber, P. Wang, G. Rizzoli, H. Zhao, S. D. Meier, D. Roth, N. Navab *et al.*, “Housecat6d—a large-scale multi-modal category level 6d object pose dataset with household objects in realistic scenarios,” *arXiv preprint arXiv:2212.10428*, 2022.
- [26] P. Z. Ramirez, A. Costanzino, F. Tosi, M. Poggi, S. Salti, S. Mattoccia, and L. Di Stefano, “Booster: a benchmark for depth from images of specular and transparent surfaces,” *IEEE Transactions on Pattern Analysis and Machine Intelligence*, vol. 46, no. 1, pp. 85–102, 2023.
- [27] K. Daniilidis, “Hand-eye calibration using dual quaternions,” *The International Journal of Robotics Research*, vol. 18, no. 3, pp. 286–298, 1999.
- [28] [Online]. Available: <https://sites.google.com/view/iccv25tricky/home>
- [29] T.-Y. Lin, M. Maire, S. Belongie, J. Hays, P. Perona, D. Ramanan, P. Dollár, and C. L. Zitnick, “Microsoft coco: Common objects in context,” in *Computer vision—ECCV 2014: 13th European conference, zurich, Switzerland, September 6–12, 2014, proceedings, part v 13*. Springer, 2014, pp. 740–755.
- [30] P. Z. Ramirez, F. Tosi, M. Poggi, S. Salti, S. Mattoccia, and L. Di Stefano, “Open challenges in deep stereo: the booster dataset,” in *Proceedings of the IEEE/CVF Conference on Computer Vision and Pattern Recognition*, 2022, pp. 21 168–21 178.
- [31] P. Z. Ramirez, F. Tosi, L. Di Stefano, R. Timofte, A. Costanzino, M. Poggi, S. Salti, S. Mattoccia, Y. Zhang, C. Wu *et al.*, “Ntire 2024 challenge on hr depth from images of specular and transparent surfaces,” in *Proceedings of the IEEE/CVF Conference on Computer Vision and Pattern Recognition*, 2024, pp. 6499–6512.
- [32] Z. Ge, S. Liu, F. Wang, Z. Li, and J. Sun, “Yolox: Exceeding yolo series in 2021,” *arXiv preprint arXiv:2107.08430*, 2021.
- [33] V. N. Nguyen, T. Groueix, G. Ponimatkin, V. Lepetit, and T. Hodan, “Cnos: A strong baseline for cad-based novel object segmentation,” in *ICCV*, 2023.
- [34] R. L. Haugaard and A. G. Buch, “Surfemb: Dense and continuous correspondence distributions for object pose estimation with learnt surface embeddings,” in *CVPR*, 2022.

- [35] J. Redmon, S. Divvala, R. Girshick, and A. Farhadi, "You only look once: Unified, real-time object detection," in *Proceedings of the IEEE conference on computer vision and pattern recognition*, 2016, pp. 779–788.
- [36] A. Kirillov, E. Mintun, N. Ravi, H. Mao, C. Rolland, L. Gustafson, T. Xiao, S. Whitehead, A. C. Berg, W.-Y. Lo *et al.*, "Segment anything," *arXiv preprint arXiv:2304.02643*, 2023.
- [37] M. Oquab, T. Darcet, T. Moutakanni, H. Vo, M. Szafraniec, V. Khalidov, P. Fernandez, D. Haziza, F. Massa, A. El-Nouby *et al.*, "Dinov2: Learning robust visual features without supervision," *arXiv preprint arXiv:2304.07193*, 2023.
- [38] A. Dosovitskiy, L. Beyer, A. Kolesnikov, D. Weissenborn, X. Zhai, T. Unterthiner, M. Dehghani, M. Minderer, G. Heigold, S. Gelly *et al.*, "An image is worth 16x16 words: Transformers for image recognition at scale," *arXiv preprint arXiv:2010.11929*, 2020.
- [39] Z. Qin, H. Yu, C. Wang, Y. Guo, Y. Peng, S. Ilic, D. Hu, and K. Xu, "Geotransformer: Fast and robust point cloud registration with geometric transformer," *IEEE Transactions on Pattern Analysis and Machine Intelligence*, vol. 45, no. 8, pp. 9806–9821, 2023.
- [40] L. Yang, B. Kang, Z. Huang, Z. Zhao, X. Xu, J. Feng, and H. Zhao, "Depth anything v2," *Advances in Neural Information Processing Systems*, vol. 37, pp. 21 875–21 911, 2024.
- [41] [Online]. Available: https://cmp.felk.cvut.cz/sixd/workshop_2025/
- [42] X. Liu, R. Zhang, C. Zhang, G. Wang, J. Tang, Z. Li, and X. Ji, "Gdrnpp: A geometry-guided and fully learning-based object pose estimator," *IEEE Transactions on Pattern Analysis and Machine Intelligence*, 2025.

Supplementary Material

XYZ-IBD: High-precision Bin-picking Dataset for Object 6D Pose Estimation Capturing Real-world Industrial Complexity

Junwen Huang Jizhong Liang Jiaqi Hu Martin Sundermeyer
Peter KT Yu Nassir Navab Benjamin Busam

A Data Splits and Challenges

A.1 Synthetic Training Data

All 15 collected industrial objects are used to generate the synthetic training dataset. We show the CAD models and the real objects for the collected industrial parts in Figure 6. For each scene, we simulate a free-fall of multiple object instances and render 25 images under varying lighting conditions and material properties. The rendering process uses the same camera intrinsics as the XYZ Robotics structured light camera. For each object, 120 scenes are rendered, resulting in approximately 3,000 bin-picking frames per object. This bin-picking synthetic dataset provides ground truth object masks, depth images and object 6D poses, therefore can be used as the training set for the depth estimation, 2D detection and pose estimation tasks. In total, the synthetic training dataset contains 45,000 RGB-D frames and occupies about 80 GB.



Figure 6: The collected industrial parts and their corresponding CAD models of XYZ-IBD dataset.

A.2 BOP Challenge 2025 - Industrial Track

Overview. XYZ-IBD dataset is one of the official industrial datasets in the BOP (Benchmark for 6D Object Pose Estimation) Challenge 2025 industrial track [3, 41]. For each of the 15 real industrial parts, we collected 5 different scenes by varying the number of instances, lighting conditions and object poses. We use 1 scene for each object as the validation set, and 4 scenes for each object as the test set. In the test set, we follow the BOP Challenge 2025’s setup and provide both single-view and multi-view evaluation protocols. For multi-view evaluation, 5 viewpoints are selected per scene based on the maximum spatial spread. One view is designated as the target view for evaluation, while the other 4 views serve as reference views. Relative camera poses among the 5 views are provided to enable multi-view methods to exploit spatial context. For single-view methods, only the target view is used. The ground truth pose of the validation set is released publicly, but the ground truth of the test set is hidden and hosted in the BOP evaluation system. The validation set size is approximately 8 GB, while the test set occupies around 3 GB.

Links. There are multiple ways to access XYZ-IBD dataset and evaluate the methods on the dataset, here we provide the links to download the data and evaluate the methods on this dataset.

- **Downloads.** The full synthetic training set, validation set and testing set of XYZ-IBD dataset are hosted on HuggingFace: <https://huggingface.co/datasets/bop-benchmark/xyzibd>.

Alternatively, users can also download the dataset from the official BOP website: <https://bop.felk.cvut.cz/datasets/>.

- **Evaluations.** To evaluate methods on XYZ-IBD, users can submit their results to the BOP evaluation server: <https://bop.felk.cvut.cz/leaderboards/>. The server supports multiple tasks on XYZ-IBD, including: Model-based 6D detection on **unseen** objects, Model-based 2D detection on **unseen** objects, Model-based 6D detection on **seen** objects, Model-based 2D detection on **unseen** objects. Users may also evaluate locally using the official toolkit: https://github.com/thodan/bop_toolkit, which includes visualizers, data loaders, and evaluation scripts for XYZ-IBD.

A.3 TRICKY Challenge 2025 – Monocular Depth Track

Overview. The XYZ-IBD dataset is also included in the TRICKY Challenge 2025 [28] (Transparent & Reflective Objects In the Wild Challenges). It uses the same real-world validation split as the BOP Challenge but selects different views from the test scenes for the monocular depth estimation task. Ground-truth depth maps are provided for both the training and validation splits, while the test set annotations remain hidden and are evaluated through the official TRICKY Challenge platform. Both TRICKY and BOP Challenges share the same synthetic training dataset.

Links. The training and validation splits for the depth estimation task can be downloaded from the official TRICKY Challenge 2025 website: <https://sites.google.com/view/iccv25tricky/home#h.h0s7c37d7fmm>

The evaluation system is hosted on the CodaLab platform: https://codalab.lisn.upsaclay.fr/competitions/22870#learn_the_details

B Implementation Details for the Baselines

All seen-object baseline methods are trained on our synthetic training dataset and evaluated on the real testing split. For all the unseen baselines, we directly use the pretrained model to infer on the testing split.

B.1 YOLOX

We train a YOLOX [32] model for object detection following the configuration used in GDRNPP [42]. Training is performed on a single NVIDIA RTX 4090 GPU with a batch size of 24 for 30 epochs. Data augmentation is applied during the first 15 epochs, consistent with the GDRNPP setup. The complete training process on the synthetic PBR dataset takes approximately 18 hours.

B.2 GDRNet

GDRNet [12] is trained on all the objects of our synthetic dataset with a batch size of 24 for 10 epochs, totaling roughly 490,000 training steps. The training is conducted on a single NVIDIA RTX 4090 GPU and completes in approximately 24 hours.

B.3 SurfEmb

SurfEmb [34] is trained on each object of our synthetic dataset with a batch size of 24 for 500,000 steps. Training is performed on a single NVIDIA RTX 4090 GPU and takes approximately 20 hours.

C More Visualizations of Data Samples

We visualize more data samples in this section. Figure 7 shows more examples for the scenes that were recorded with the XYZ camera, and Figure 8 shows more examples from the RealSense camera. We compare our dataset with other BOP datasets with the instance distribution in Figure 9. The dataset follows the BOP dataset format as shown in Figure 10.

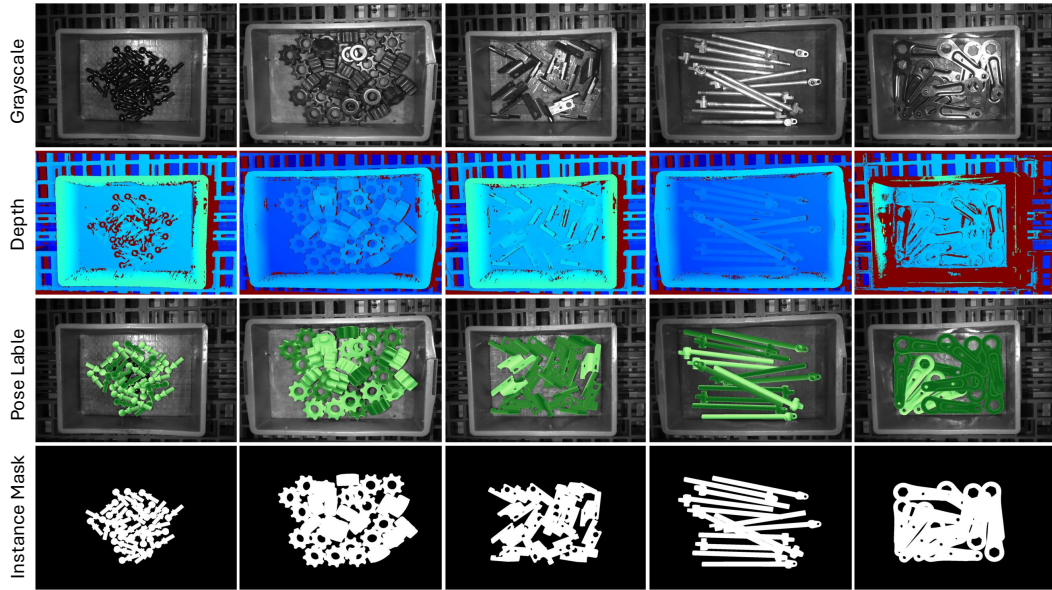


Figure 7: More data samples from the XYZ camera.

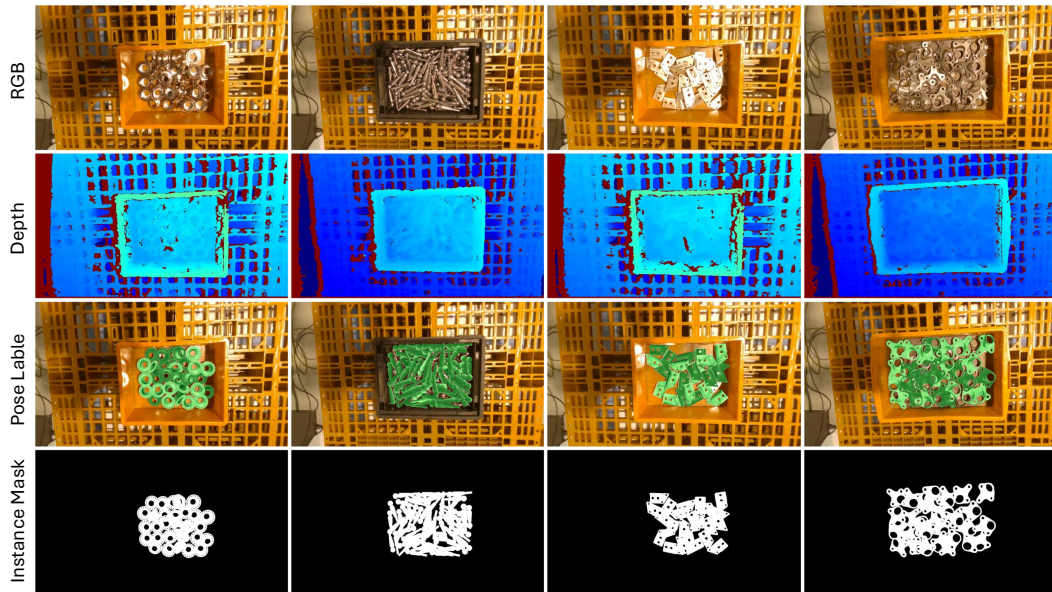


Figure 8: More data samples from the RealSense camera.

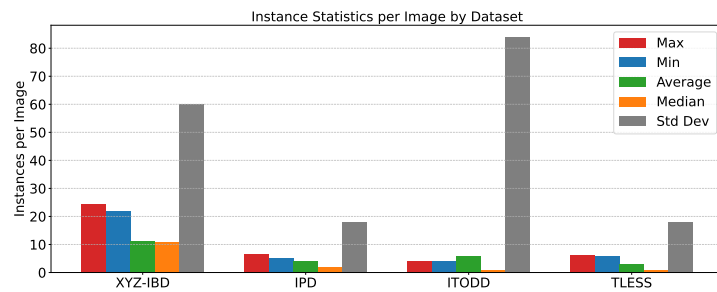


Figure 9: The instance distribution of the BOP industrial datasets.

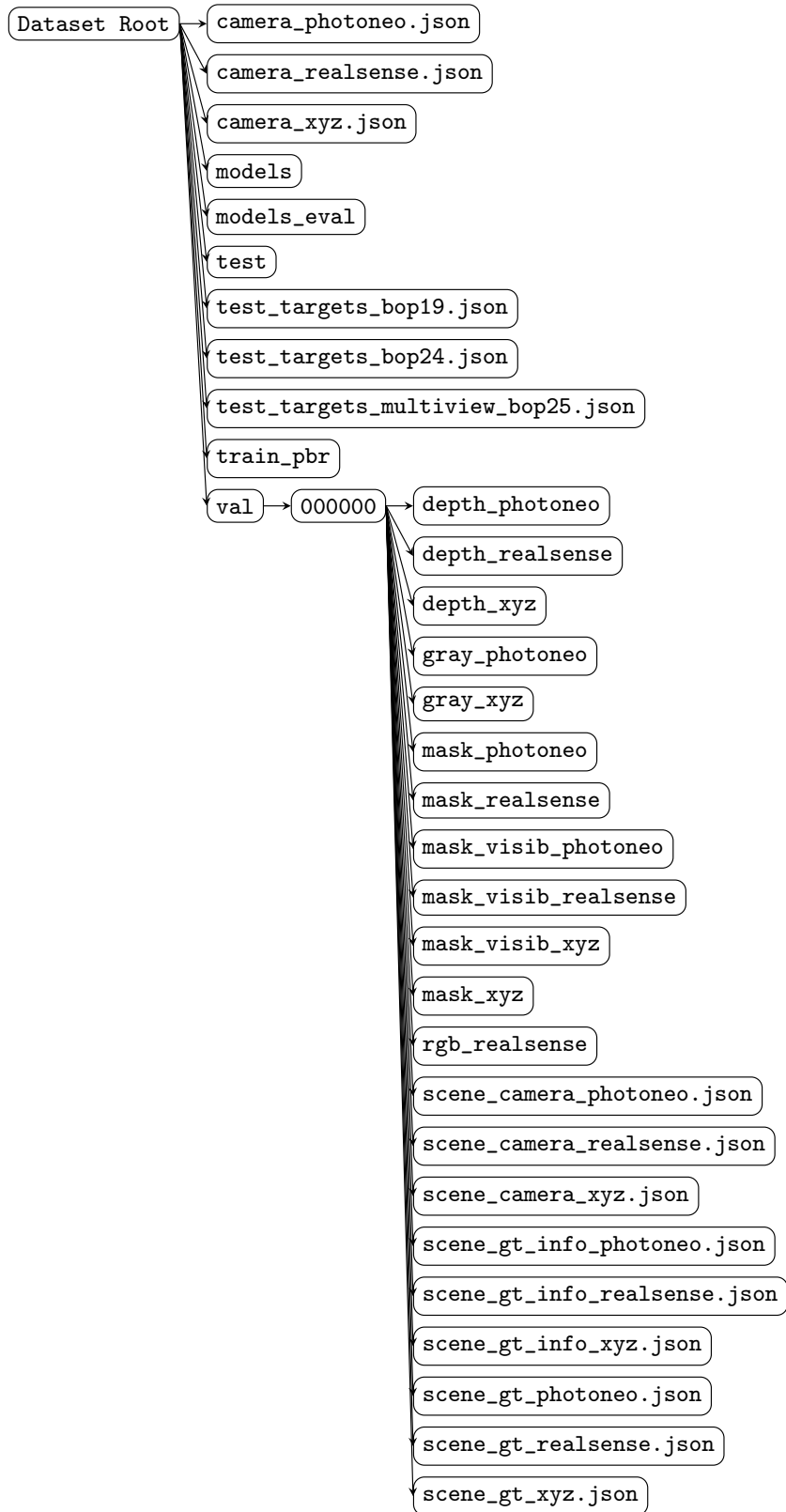


Figure 10: Directory structure of the dataset.